Chapter 3

Stability of membrane bound reactions

3.1 Introduction

A basic task of cells is to respond to inner and outer stimuli which involves sequences of chemical reactions forming the signaling pathway. Some of these reactions take place in the cytosol between dissolved partners. Others occur in the plasma or organellic membranes. A third kind happens between cytosolic molecules and membrane bound reaction partners. Frequently these reactions involve only a small part of the membrane at a time because a cell does not only interpret the total amount of additional substances, but also the precise location of its production. A well known example for this is the formation of cyclic adenosine monophosphate (cAMP). Here dissolved adenosine trisphosphate (ATP) binds to adenylate cylcase that is fixed in the plasma membrane. Depending on where cAMP is fabricated it may trigger a break down of glycogen to glycose or the expression of a gene (Alberts et al. 1994). The initiation of ion fluxes through ion channels by ligand binding can as well be perceived as a localized reaction.

Generally not all molecules residing in the membrane patch take part in the reaction, but only those which are activated. Although the activating mechanism differs among membrane bound processes it is a ubiquitous property. Therefore we may refer to the molecules in the particular membrane area participating in a reaction as active elements. A single cluster with a few tens of them is the focus of this chapter.

The small number of active elements in a cluster entails small cluster areas. This strong localization of the reactions causes large gradients of produced species. It imposes limits on the reaction arising from diffusion of dissolved reaction partners

toward or away from the cluster. Here, we will model the dynamics of an active cluster taking diffusion of dissolved reaction partners into account.

Ca^{2+} signaling has a prominent role among the above mentioned signaling tasks of a cell (Berridge et al. 2000). In the following the IP_3 receptor will serve as an illustrative example. As opposed to chapter 1 more details about the dynamical behavior of the receptor are required. Especially the impact of the cytosolic Ca^{2+} concentration on the open probability needs further consideration. A moderate increase raises the tendency to release calcium, whereas a high Ca^{2+} concentration causes inhibition and closes the channel. Thus the channel releases what controls its state.

The feedback of Ca^{2+} on the channel dynamics becomes even more relevant when we take the spatial organization of IP_3 receptors into account. Generically they form clusters that are randomly distributed on the ER membrane. The typical inter cluster distance is 2-7μm (Marchant and Parker 2001). The number of IP_3Rs within a cluster has not been experimentally established yet. However, Swillens et. al (Swillens et al. 1999) estimate that a a cluster comprises 5 to 40 channels. As a single IP_3R with all four subunits measures 18nm across we arrive at a cluster diameter of 60-100nm. Therefore IP_3 receptors are tightly coupled by diffusion within a cluster because the Ca^{2+} concentration does not decay on this length scale. On the other hand coupling between adjacent clusters is only weak.

The spatial heterogeneity of Ca^{2+} release sites leads to huge gradients. The simulations in chapter 1 of Ca^{2+} liberation close to the experimental situation show Ca^{2+} concentrations of 25-170μM at the center of a cluster. That is 3-4 orders of magnitude larger than the base level. At the same time the concentration increases only 1-2 times base level at neighboring clusters. This wide range of Ca^{2+} concentrations is naturally reflected in the properties of an IP_3R. Experimental observations like propagating waves and theoretical considerations indicate that the sensitivity of the activating Ca^{2+} dependence of the opening probability on Ca^{2+} is tuned to concentration levels close to the resting level. On contrast Ca^{2+} inhibition shows half maximum values of several μM. These responses to different Ca^{2+} concentrations have to be dealt with when designing realistic models.

The small number of elements per cluster may necessitate stochastic approaches which has been carried out for intracellular Ca^{2+} dynamics (Falcke et al. 2000b, Falcke 2003b, Bär et al. 2000). They showed spatial and temporal structures even with parameters providing a non-oscillatory or non-excitable deterministic regime. The transition from deterministic to stochastic models was accompanied by a transition from continuous to spatially discrete models. In this chapter we focus on the deterministic limit of a single cluster to elucidate the loss of the

oscillatory regime in going from the stochastic to the deterministic approach.

3.2 General Model

The state of active elements can be described as either activated or deactivated. As their number per cluster is rather small and as they are tightly packed, each element occupies a non negligible spatial fraction. Therefore the state of a cluster is well characterized by the area occupied by activated units. We refer to it as the active area of a cluster. Usually this is not a connected region. Nevertheless we merge the area of all activated elements to one concentric patch. Its size equals the sum of the areas of all activated units and its radius is denoted by a. This can be applied if the diffusion length of the diffusing species is larger than the cluster size. The procedure follows a result by Swillens and Dupont (Swillens et al. 1999). They showed that the dynamics of an IP_3R cluster does not change when the spatial arrangement of the receptors is neglected. A change in the number of activated elements thus implies an alteration of the size of the active area. If all elements are deactivated a equals zero. The maximum value a_0 is taken when all units are activated.

a_0 is the maximal radius of a sphere to which the active elements are restricted in our model. A typical value for a_0 is tens of nanometers. Another sphere with a radius $b = 5 - 100\mu m$ surrounds the active region concentrically. It represents the environment of a cluster.

Throughout the two spherical compartments m chemical species diffuse. They are described by the concentration fields $c(r,t) := \{c_1(r,t), \ldots, c_m(r,t)\}$. Their dynamics is of the general form as shown in equation (3.1).

$$\dot{c} = D\nabla_r^2 c + f_1(c)\Theta\left(a - r\right) + f_2(c)\Theta\left(r - a\right) \ . \tag{3.1}$$

Here ∇_r^2 denotes the radial part of the Laplacian in three dimensions. $\Theta(x)$ with $\Theta(x) = 1$ for $x \geq 0$, $\Theta(x) = 0$ otherwise is for the Heaviside step function. The functions f_1 and f_2 include the details of the dynamics for $r \leq a$ and $r > a$ respectively. Most commonly, f_1 is dominated by the production of the species, whereas f_2 controlls mere consumption.

These chemical species react with the active elements thus controlling their state. Usually there are several binding sites per element which implies numerous internal configurations. We refer to the variables describing the state of the active elements as gating variables. Let n be the number of states then $p_i, i = 1, \ldots, n$ denotes the fraction of elements in the state i. We describe the dynamics of the

gating variables by the general equation

$$\dot{p}_i = g_i(c, p_1, \ldots, p_n)\,, \quad i = 1, \ldots, n\,. \tag{3.2}$$

The fraction of activated elements is deduced from the gating variables. Consequently they determine the radius of the active area as in equation (3.3). We here include a dependence on the chemical species as well to account for the most general case.

$$a = f(c(a), p_1(a), \ldots, p_n(a))\,. \tag{3.3}$$

The values of the concentration fields and of the gating variables do not vary significantly within a cluster because the diffusion lengths are larger than the radius of the active area. Therefore we can pick a typical value to compute a. We choose the boundary of the cluster which turns equation (3.3) into an implicit expression for a.

We start our analysis by calculating the stationary solutions of equations (3.1) and (3.2):

$$0 = D\nabla_r^2 c + f_1(c)\Theta\left(\bar{a} - r\right) + f_2(c)\Theta\left(r - \bar{a}\right)) \tag{3.4a}$$

$$0 = g_i(c, p_1, \ldots, p_n)\,, \quad i = 1, \ldots, n\,. \tag{3.4b}$$

Due to the Heaviside function equation (3.4a) can be treated separately for $r < \bar{a}$ and $r > \bar{a}$. $\bar{a}$ denotes the stationary value of the active area. As we demand the concentration profiles to be C^1 functions with respect to r, the matching conditions for the stationary solutions $\bar{c}$ are $\bar{c}_i(\bar{a}) = \bar{c}_o(\bar{a})$ and $\bar{c}_i'(\bar{a}) = \bar{c}_o'(\bar{a})$. The prime denotes the derivative with respect to r, the subscripts i and o indicate the inner and outer solution, respectively. The values of $\bar{a}$ are obtained from equation (3.3) after inserting the solutions of equation (3.4). In figure 3.5 we show a graphical method to determine $\bar{a}$. The dotted line indicates the bisection line whereas the full lines represent the right hand side of equation (3.3) for a specific model (see below). Upon changing one parameter the curve of f is shifted. It results in a change of the number of fixed points given by the intersections. The existence of a saddle node bifurcation is easily deduced from such a plot. It occurs when f touches the bisection line. This is equivalent to the condition $f'(a) = 1$.

Knowing the stationary points $(\bar{c}, \bar{a})$ we investigate their stability. A linearization of the reaction diffusion dynamics in (3.1) results in the equation

$$\begin{aligned} \dot{y} = {} & D\nabla_r^2 y + \left\{f_1(\bar{c}) - f_2(\bar{c})\right\}\delta_D(\bar{a} - r)\delta a\,(y, z) \\ & + \left\{\frac{\partial f_{1i}}{\partial c_j}(\bar{c})\Theta(\bar{a} - r) + \frac{\partial f_{2i}}{\partial c_j}(\bar{c})\Theta(r - \bar{a})\right\} \cdot y \end{aligned} \tag{3.5}$$

We define $y := \delta c$ and $z := \delta p$. With δ_D we denote Dirac's delta function. Although a is not a dynamical variable in our model it still changes in time. This is a consequence of equation (3.3) as a is computed from the evolving concentration fields and gating variables. a can be written as $a = \bar{a} + \delta a$ with $\delta a = \delta a(y, z)$. To evaluate δa from equation (3.3) we expand the expression

$$\bar{a} + \delta a = f\left(\bar{c}(r) + y(r), \bar{p}(r) + z(r)\right)\Big|_{r=\bar{a}+\delta a} \tag{3.6}$$

to linear order. We find

$$\delta a = \frac{\sum_{i=1}^{m} \frac{\partial f}{\partial c_i} y(\bar{a}) + \sum_{i=1}^{n} \frac{\partial f}{\partial p_i} z_i(\bar{a})}{1 - \sum_{i=1}^{m} \frac{\partial f}{\partial c_i} \frac{\partial \bar{c}_i}{\partial r}(\bar{a}) - \sum_{i=1}^{n} \frac{\partial f}{\partial p_i} \frac{\partial \bar{p}_i}{\partial r}(\bar{a})} \,. \tag{3.7}$$

The derivatives of f have to be taken at $(\bar{c}(\bar{a}), \bar{p}(\bar{a}))$. The denominator arises only because of the evaluation of f at $r = a$.

When we combine y and z to an $n + m$ dimensional vector x the linearized equations can be cast into a matrix form $\dot{x} = Mx$ with

$$x = \begin{pmatrix} y \\ z \end{pmatrix} \,, \quad M = \begin{pmatrix} A_1 & 0 \\ B & A_2 \end{pmatrix} \,. \tag{3.8}$$

A_1 is an m dimensional quadratic matrix corresponding to equation (3.5). The quadratic matrix A_2 has the dimension $\dim A_2 = n$ and $B \in \mathbb{R}^{n \times m}$. They refer to the linearization of the gating dynamics. If M can be diagonalized, the general solution for the equation $\dot{x} = Mx$ is given by a linear combination of terms $v_i \exp(w_i t)$. v_i represents an eigenvector of M and w_i the corresponding eigenvalue. Thus, the linear stability is uniquely determined by the eigenvalues of M. The computation of the eigenvalues begins with A_2. The gating dynamics of the spatially fixed active elements is described by rate equations, so that the Frobenius Perron theorem assures that A_2 can be diagonalized. Additionally, all eigenvalues λ_i of A_2 are real with $\max \lambda_i = 0$ (Horn and Johnson 1999). On the one hand the structure of M entails $\{\lambda_i\} \subset \{w_i\}$, i.e. the eigenvalues of M include those of A_2. On the other hand the eigenvector q_i corresponding to the eigenvalue λ_i is of the form $(0, \ldots, 0, \tilde{q}_i)^t$ with $\dim \tilde{q}_i = n$. This has two important consequences. Due to $\lambda_i \leq 0$ the gating variables $\{p\}$ whose linear disturbance is denoted by z do not contribute to any linear instability. The only mechanism that can induce an instability comes from the dynamics of the diffusing species c. The special form of the eigenvectors q_i imposes that the dynamics of y does not depend on the eigenvalues $\{\lambda_i\}$. All information about the linear stability of the dynamics of the diffusing species c and the non diffusing active elements

characterized by the gating variables p is contained in equation (3.5). This is one of the advantages of the procedure we have chosen. Especially in the case of a single diffusing species a far reaching analytical treatment is feasible. We show this in more detail in section 3.4.

As it is for the fixed points, equation (3.5) can be solved separately for $r < \bar{a}$ and $r > \bar{a}$. The matching conditions are slightly different than those for the stationary profiles. The both share continuity at $r = \bar{a}$. This equals $y_i(\bar{a}) = y_o(\bar{a})$. However, the first derivate jumps at $r = \bar{a}$ according to

$$\left[\frac{dy_o}{dr} - \frac{dy_i}{dr} + \frac{f_1(\bar{c}) - f_2(\bar{c})}{D}\delta a\,(y,z)\right]_{\bar{a}} = 0\,. \tag{3.9}$$

This is a consequence of the δ-function in equation (3.5). Multiplying the linearized equation with r^2 and integrating over r yields equation (3.9). Note that $\nabla_r^2 = 1/r^2 d_r r^2 d_r$ in three dimensions.

The continuity at $\bar{a}$ and equation (3.9) fix the still undetermined coefficients of y. By construction the resulting system of equations is homogeneous. Therefore it has a non trivial solution only if the determinant vanishes. This yields an implicit equation for the eigenvalues of the concentration fields and thus determines their linear stability.

3.3 The De Young Keizer model

The general ideas of section 3.2 will be illustrated below with IP_3 induced Ca^{2+} liberation from the ER. This requires a closer look on the IP_3 receptor. Measurements on the flux properties have revealed a tetrameric structure (Bezprozvanny et al. 1991, Watras et al. 1991). This has been confirmed by cryo-electron microscopy on single IP_3Rs (Jiang et al. 2002). The four subunits are clearly depicted in figure 3.1.

It is known that a subunit expresses binding sites for Ca^{2+} and IP_3. However, the exact number of binding sites is still under investigation. Based on the results of Bezprozvanny et al. (Bezprozvanny et al. 1991) de Young and Keizer proposed a model for a single subunit (De Young and Keizer 1992). It consists of three binding sites: an activating and an inhibitory Ca^{2+} binding site as well as an activating IP_3 binding site. Therefore the state of a subunit can be specified by a binary triplet ijk. The first index represents the IP_3 binding site, the second the Ca^{2+} activating and the last the Ca^{2+} inhibiting binding site. An index equals 1 when a site is occupied and 0 otherwise. Hence the state 110 refers to IP_3 and Ca^{2+} bound to the activating sites, respectively, and no Ca^{2+} attached to

Figure 3.1: Cryo-electron microscopic images of purified type I IP_3 receptor from mouse cerebellum. Figure from (Jiang et al. 2002).

the inhibiting binding site. The resulting eight states of a subunit are shown in figure 3.2. The binding rate constants for IP_3 activation are given by a_1 and a_3, whereas a_2 and a_4 refer to Ca^{2+} inhibition. Ca^{2+} activation is controlled by a_5. The dissociation rates for the above processes are denoted by b_1 through b_5.

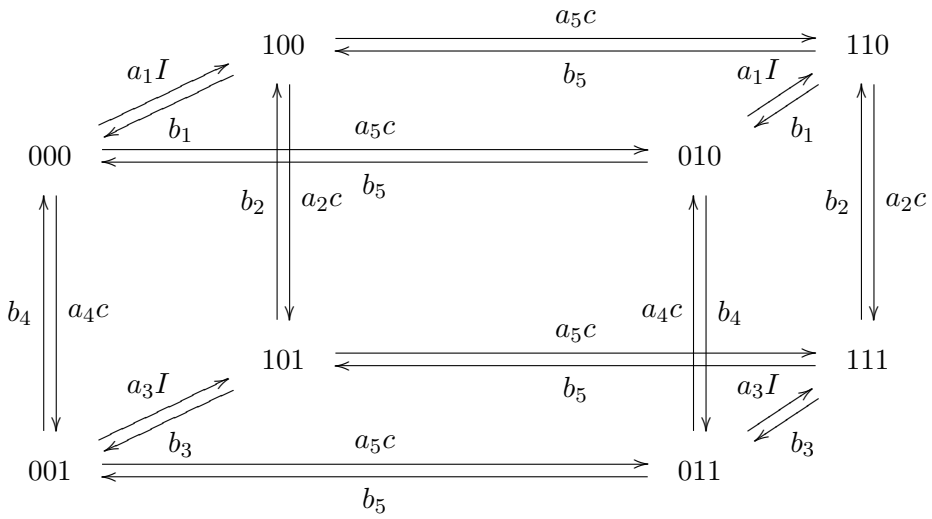

Figure 3.2: Transition scheme of the De Young Keizer model

The reactions that occur at a subunit are binding and unbinding of Ca^{2+} and IP_3. They determine the state of one subunit. In an ensemble of subunits these processes lead to a fraction p_{ijk} of subunits in a state ijk. If the ensemble is large enough and homogeneous, these fractions can be described by rate equations.

For instance, the time evolution of p_{110} is governed by

$$\dot{p}_{110} = -\left[b_5 + a_2 c + b_1\right] p_{110} + a_5 c p_{100} + b_2 p_{111} + a_1 I p_{010}\,, \tag{3.10}$$

with I being the IP_3 concentration and c the Ca^{2+} concentration. The negative term represents the processes that reduce the value of p_{110}. This can result from unbinding of IP_3 with rate b_1, unbinding from the activating Ca^{2+} site with rate b_5 and binding to the inhibiting Ca^{2+} binding site with rate $a_2 c$. The remaining three terms controll the increase of p_{110}. This happens for example through binding with rate $a_5 c$ to the activating Ca^{2+} site of a subunit that is in the state 1o0. Together with the remaining seven rate equations the state of the ensemble is fully characterized. We may discard one of these equations and use instead the conservation law

$$\sum_{\{ijk\}\in[0,1]^3} p_{ijk} = 1\,. \tag{3.11}$$

It states that each subunit belongs to one of the fractions p_{ijk} and that the number of subunits is conserved. In general the Ca^{2+} concentration is not constant in time, so that a closed solution for the fractions p_{ijk} is not accessible. However, we can compute the stationary values analytically. They read

$$\bar{p}_{000} = d_1 d_2 d_5 \gamma_1\,, \qquad \bar{p}_{100} = d_2 d_5 I \gamma_1\,, \tag{3.12a}$$

$$\bar{p}_{010} = d_1 d_2 \bar{c} \gamma_1\,, \qquad \bar{p}_{001} = d_3 d_5 \bar{c} \gamma_1\,, \tag{3.12b}$$

$$\bar{p}_{011} = d_3 \bar{c}^2 \gamma_1\,, \qquad \bar{p}_{101} = d_5 \bar{c} I \gamma_1\,, \tag{3.12c}$$

$$\bar{p}_{110} = d_2 \bar{c} I \gamma_1\,, \qquad \bar{p}_{111} = \bar{c}^2 I \gamma_1\,, \tag{3.12d}$$

with $\gamma_1^{-1} = (\bar{c}+d_5)(d_1 d_2 + \bar{c} d_3 + \bar{c} I + d_2 I)$. Here $d_i := b_i/a_i$ denotes the dissociation constants for IP_3 activation, Ca^{2+} activation and inhibition, respectively.

Despite the success that the De Young Keizer (DK) model has earned in the past, the seven dimensional phase space of the gating variables does not allow a straightforward study of the dynamics. Besides the stationary states, all results for the DK model have been obtained by numerical integrations. The ambitions to gain further insights into intracellular Ca^{2+} dynamics based on the IP_3 receptor have led to several approximations of the DK model. On the one hand numerical investigations could be sped up. On the other hand a broader analytical treatment was feasible. In the remainder of this section we will cover three simplifications of the DK model. We will show that the stationary values of the gating variables do not depend on the approximation. Hence all expressions that include stationary values of the gating variables only do not differ. This will prove helpful in section 3.4.

De Young and Keizer assume that the dynamics of IP_3-association and dissociation is much faster than the dynamics of Ca^{2+}-binding and unbinding. Therefore we eliminate the IP_3 dynamics by assuming that it is always in its stationary state. Given a pair of states $(1ij, 0ij)$ the fraction $p_{1ij}/p_{0ij} = \beta_{ij}$ remains constant. This can be visualized by merging the back side of the cube in figure 3.2 with the front panel. The eight states of the DK model are reduced to four lumped states $p_{ij} := p_{0ij} + p_{1ij}$ (Falcke et al. 2000b). The gating scheme is depicted in figure 3.3.

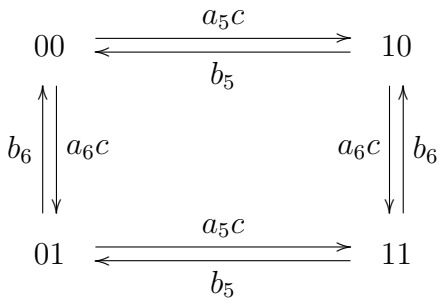

Figure 3.3: Transition scheme for the lumped states of the IP_3 receptor.

The rate equations of the lumped states follow from those of the DK model. Alternatively, we may employ figure 3.3 and find for example

$$\dot{p}_{10} = -\left(a_6 c + b_5\right) p_{10} + b_6 p_{11} + a_5 c p_{00} \,. \tag{3.13}$$

A general solution to the four rate equations cannot be computed analytically because of the time dependent Ca^{2+} concentration. Yet, the stationary solutions are accessible as

$$\bar{p}_{00} = d_5 d_6 \gamma_2 \,, \qquad \bar{p}_{01} = d_5 \bar{c} \gamma_2 \,, \tag{3.14a}$$

$$\bar{p}_{10} = d_6 \bar{c} \gamma_2 \,, \qquad \bar{p}_{11} = \bar{c}^2 \gamma_2 \,, \tag{3.14b}$$

with $\gamma_2^{-1} = (\bar{c} + d_5)(\bar{c} + d_6)$ and $d_6 = d_2(I + d_1)/(I + d_3)$. Evaluating the β_{ij} and using the lumped state definition entails that equations (3.14) lead to the same stationary values $\bar{p}_{ijk}$ as the DK model e.g.

$$\bar{p}^{lu}_{110} = \frac{I}{I + d_d} \bar{p}_{10} = \bar{p}^{DK}_{110} \,. \tag{3.15}$$

The gating dynamics can be even further simplified when we consider Ca^{2+} activation and Ca^{2+} inhibition more closely. Experiments show that the inhibitory

processes may be much slower than the activating ones. It is possible to eliminate Ca^{2+} activation adiabatically under these circumstances. Then it is characterized by the stationary states of the Ca^{2+} activating reactions. The only time dependent variable that remains is the fraction of subunits that are not inhibited yet. It is denoted by p_h with $h = 000 + 100 + 010 + 110$. h corresponds to the states in the upper plane of the cube in figure 3.2. In an ostensive way the introduction of h mimics to subsume the four states in this upper plane to a single state. At the same time all dynamics linking these states are assumed to have equilibrated. Li and Rinzel have performed a systematic reduction of the DK model to the dynamics of p_h (Li and Rinzel 1994). They applied a two time scale analysis. Another approach is to take the pictorial idea of h literally. This leads to

$$\begin{aligned}\dot{p}_h = &-\left[(m_1{+}m_2)a_2c + (m_3{+}m_4)a_4c\right]p_h + \left[(m_5{+}m_6)b_2 + (m_7{+}m_8)b_5\right]p_{\bar{h}} \\ &- a_6cp_h + b_6p_{\bar{h}}\,.\end{aligned} \tag{3.16}$$

with $\bar{h} := 001 + 011 + 101 + 111$, $a_6 = (d_1a_4 + a_2I)/(I + d_1)$ and $b_6 = (b_4d_3 + b_2I)/(I + d_3)$. The m_i are given by

$$m_1 = \frac{I}{I+d_1}\frac{c}{c+d_5}\,, \quad m_2 = \frac{I}{I+d_1}\frac{d_5}{c+d_5} \tag{3.17a}$$

$$m_3 = \frac{d_1}{I+d_1}\frac{c}{c+d_5}\,, \quad m_4 = \frac{d_1}{I+d_1}\frac{d_5}{c+d_5} \tag{3.17b}$$

$$m_5 = \frac{I}{I+d_3}\frac{c}{c+d_5}\,, \quad m_6 = \frac{I}{I+d_3}\frac{d_5}{c+d_5} \tag{3.17c}$$

$$m_7 = \frac{d_3}{I+d_3}\frac{c}{c+d_5}\,, \quad m_8 = \frac{d_3}{I+d_3}\frac{d_5}{c+d_5}\,. \tag{3.17d}$$

The values of the m_i mirror the equilibria of the reactions between the states in the lower and upper plane depicted in figure 3.2, respectively. As illustration we derive m_1. Suppose we start in the upper plane. The Ca^{2+} activating processes have equilibrated, so that the probability to be in one of the states at the right edge, i.e. 110 and 010, is $c_5/(d_5{+}c)$. IP_3 binding and unbinding between these has reached its stationary value. The fraction p_{110}/p_{010} is constant and the probability to be in 110 is $I/(I + d_1)$. The product of the above two probabilities just equals m_1. The other seven constants are calculated in the same fashion.

Sometimes the rates in equation (3.16) are given as $a_6 = a_2$ and $b_6 = b_2(I + d_1)/(I + d_3)$. This follows from the above expressions when the detailed balance condition $d_4 = d_1d_2/d_3$ and the symmetry assumption of the Ca^{2+} inhibiting processes, $a_2 = a_4$, is applied. The fixed point of equation (3.16) is

$$\bar{p}_h = \frac{d_6}{d_6 + \bar{c}}\,. \tag{3.18}$$

As for the lumped states the stationary values $\bar{p}_{ikj}$ calculated from the Li Rinzel model equal those of De Young and Keizer. For instance we arrive at

$$\bar{p}_{110}^{LR} = \frac{I}{I+d_1}\frac{\bar{c}}{\bar{c}+d_5}\bar{p}_h = \bar{p}_{110}^{DK}\,. \tag{3.19}$$

Although the Li Rinzel model is often implemented due to its simplicity, averaging all Ca^{2+} activating processes can be a too strong approximation. This holds in particular when fluctuations in the Ca^{2+} activating processes have to be taken into account. Averaging destroys the impact of these fluctuations. We will show in chapter 3 that fluctuations in the Ca^{2+} activation essentially shape the behavior of a single IP_3R cluster. This leads to the set up of a model that interpolates between the four lumped states and the Li Rinzel model. Its state scheme is depicted in figure 3.4. We keep the activation process between the states 00 and 10, but combine the states 11 and 01 into the state $\bar{h}$.

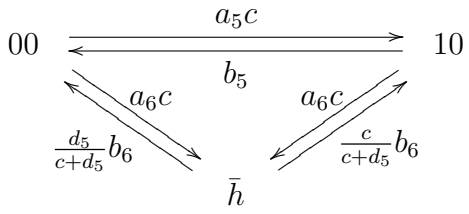

Figure 3.4: Transition scheme for a three state model of the IP_3 receptor.

The reason for this choice lies in the prominent role that the state 110 plays in the dynamics of an IP_3 receptor. When at least three subunits are in this state the IP_3 receptor channel opens and Ca^{2+} flows from the ER to the cytosol (Bezprozvanny et al. 1991). Therefore p_{110} is called the fraction of active subunits. The larger p_{110} the higher the probability for an IP_3R to open. The above model incorporates all essential transitions that change p_{110} and hence the Ca^{2+} concentration. At the same time it is compact enough for an analytical investigation as demonstrated in chapter 3. The rate equations associated with the gating scheme in figure 3.4 are

$$\frac{\partial p_{10}}{\partial t} = -\,p_{10}(a_5c + a_6c + b_5) + p_{\bar{h}}\left(\frac{b_6c}{c+d_5} - a_5c\right) + a_5c\,, \tag{3.20a}$$

$$\frac{\partial p_{\bar{h}}}{\partial t} = -\,(a_6c + b_6)p_{\bar{h}} + a_6c\,. \tag{3.20b}$$

For the stationary states we find

$$\bar{p}_{10} = \frac{d_6c}{(c+d_5)(c+d_6)}\,, \qquad \bar{p}_{\bar{h}} = \frac{c}{c+d_6}\,. \tag{3.21}$$

We here recover the stationary value $\bar{p}_{10}$ for the lumped states. Employing equation (3.18) we see that $\bar{p}_h + \bar{p}_{\bar{h}} = 1$. It is consistent with the definition of h and $\bar{h}$, because $\bar{h}$ is the complement of h with respect to the states of the DK model. We subsume that all gating schemes yield the same fixed points. Thus, as long as we are interested in quantities that depend on stationary values only, all of the above models give the same results.

Rate equations like equations (3.10) and (3.20) represent a macroscopic view. They correspond to averages and only hold in the limit of large numbers of subunits. However, a cluster of IP_3 receptors contains approximately 25 channels only. Therefore fluctuations must not be neglected any more as with equations (3.10) and (3.20). The correct description is then given by master equations. For illustrative purpose we consider the Li-Rinzel model. Let N be the total number of subunits and $P(n,t)$ the probability to find n subunits in the state h at time t. Then the probability obeys the differential equation

$$\begin{aligned}\dot{P}(n,t) =&[N-(n-1)]b_6P(n-1,t) + (n+1)a_6cP(n+1,t)\\ &- [na_6c + (N-n)b_6]P(n,t)\end{aligned} \tag{3.22}$$

The last line represents the loss processes from the state of n subunits that are not inhibited yet. Either one of them binds a Ca^{2+} ion to the inhibitory binding site with rate a_6c or a Ca^{2+} ion dissociates from one of the (N-n) inhibited subunits with rate b_6. When $(n+1)$ subunits are in the state h then binding of Ca^{2+} to one of the $(n+1)$ inhibition binding sites results in n subunits that are not inhibited yet. This process happens with the rate $a_6c(n+1)$. The first expression in the first line is the transition from $(n-1)$ to n subunits. Taking the continuous limit $N \to \infty, n \to \infty$ we obtain the rate equation (3.16) again. This establishes the connection between the microscopic and macroscopic view.

3.4 Calcium dynamics

We now apply the method of section 3.2 to the dynamics of cytosolic calcium as a prototypic model system. The cytosolic Ca^{2+} concentration c is governed by

$$\dot{c} = D\nabla^2 c + k_l(E-c) - k_p c + k_c(E-c)\Theta(a-r)\,. \tag{3.23}$$

The constants D and E denote the diffusion coefficient of Ca^{2+} in the cytosol and the Ca^{2+} concentration in the ER, respectively. The term $k_l(E-c)$ refers to a leak current whereas $k_p c$ describes the calcium uptake by the ER through sarcoendoplasmic reticulum calcium ATPase (SERCA) pumps. Although it would

be more realistic to model SERCAs by a Hill equation with coefficient 2, we approximate them by a linear expression for the sake of an analytical treatment. The last term in equation (3.23) corresponds to the flux of Ca^{2+} through IP_3 receptor channels. They represent the active elements. If not stated otherwise we employ the lumped states introduced in section 3.3 as a model for a single subunit of the IP_3 receptor. Therefore, we couple equation (3.23) to the dynamics of the gating variables $\{p_{00}, p_{01}, p_{10}, p_{11}\}$ via

$$\begin{pmatrix} \dot{p}_{00} \\ \dot{p}_{01} \\ \dot{p}_{10} \\ \dot{p}_{11} \end{pmatrix} = \begin{pmatrix} -(a_5+a_6)c & b_6 & b_5 & 0 \\ a_6 c & -(a_5 c + b_6) & 0 & b_5 \\ a_5 c & 0 & -(b_5 + a_6 c) & b_6 \\ 0 & a_5 c & a_6 c & -(b_5+b_6) \end{pmatrix} \begin{pmatrix} p_{00} \\ p_{01} \\ p_{10} \\ p_{11} \end{pmatrix} . \quad (3.24)$$

The form of the four rate equations stems from the structure of the gating dynamics of the lumped states. The latter is depicted in figure 3.3. The interpretation of equation (3.24) resembles that of equation (3.13).

In this section we will study the linear stability of equations (3.23) and (3.24). The general discussion in section 3.2 has elucidated that a linear instability can only occur through the eigenvalues associated with the Ca^{2+} concentration. Therefore, we focus on equation (3.23). We will show that the details of the gating dynamics enter late in the linear stability analysis. Most of the procedure does not depend on the specific model for an IP_3R subunit. This singles out the current method from previous approaches to IP_3 mediated Ca^{2+} liberation. Moreover, it holds for any membrane bound reaction that can be cast into the above form.

The transfer of the approach to membrane reactions is straightforward: simply replace the term describing the release current in (3.23) by an expression for the production of the diffusing species and the uptake term by their consumption dynamics. The gating variables of the channel are the variables characterizing the state of the membrane bound reaction partner.

In the DK model and all its approximations a subunit is activated when IP_3 is bound and the activating Ca^{2+} site is ligated (see section 3.3). The fraction of activated subunits is p_{110}. Thus the probability to find a conducting IP_3R is given by $4p_{110}^3 - 3p_{110}^4$ because a channel is open when at least three out of four subunits are activated. The size of the active area is set to a fraction of its maximal value corresponding to the above probability. Hence the radius a of the source area is

$$a = a_0 p_{110} \sqrt[3]{4 - 3p_{110}} \, . \quad (3.25)$$

In accordance with equation (3.3) we refer to the right hand side of (3.25) as f in the following.

Our investigations of the Ca^{2+} dynamics start with the stationary solution of (3.23):

$$\begin{aligned}\bar{c}(r) = &\left\{ \bar{B}(a)\frac{\exp(-\bar{k}_2 r)}{r} + \frac{k_l E}{k_l + k_p} \right\} \Theta(r-a) \\ &+ \left\{ \bar{A}(a)\frac{\sinh(\bar{k}_1 r)}{r} + \frac{(k_l + k_c)E}{k_l + k_p + k_c} \right\} \Theta(a-r)\end{aligned} \tag{3.26}$$

with

$$\bar{A}(a) = \frac{k(\bar{k}_2 a + 1)}{\cosh(\bar{k}_1 a)\bar{k}_1 + \sinh(\bar{k}_1 a)\bar{k}_2}\,,$$

$$\bar{B}(a) = \frac{k(\sinh(\bar{k}_1 a) - \cosh(\bar{k}_1 a)\bar{k}_1 a)}{\exp(-\bar{k}_2 a)(\cosh(\bar{k}_1 a)\bar{k}_1 + \sinh(\bar{k}_1 a)\bar{k}_2)}\,,$$

$$k = \frac{-k_c k_p E}{(k_l + k_p + k_c)(k_l + k_p)}$$

and

$$\bar{k}_1 = \sqrt{\frac{k_l + k_p + k_c}{D}}\,, \qquad \bar{k}_2 = \sqrt{\frac{k_l + k_p}{D}}\,. \tag{3.27}$$

We applied $c'(r) = 0$ and $c(b) = k_l E/(k_l + k_p)$ as boundary conditions. The latter complies with the base level of the system. The only gating variable that enters the computation of the stationary value $\bar{c}$ is p_{110} due to equation (3.25). According to equation (3.12) $\bar{p}_{110}$ in dependence on $\bar{c}$ and the IP_3 concentration I reads

$$\bar{p}_{110} = \frac{d_2 I \bar{c}(\bar{a})}{(\bar{c}(\bar{a}) + d_5)(d_1 d_2 + \bar{c}(\bar{a})d_3 + \bar{c}(\bar{a})I + d_2 I)}\,. \tag{3.28}$$

Inserting $\bar{p}_{110}$ into equation (3.25) determines the stationary values of a. They correspond to the intersections of the dotted bisection line and the curve of f depicted as solid line in figure 3.5. When we increase the IP_3 concentration I the curve of f is shifted upwards. Although $\partial f/\partial I \geq 0$ always holds, the effect on the number of stationary points depends on the parameter values. For those chosen in figure 3.5 there is one fixed point at low I. We find three stationary values at an intermediate regime and one at high IP_3 concentrations. Thus two saddle node bifurcations occur upon increasing I. As demonstrated below, one fixed point for the whole range of IP_3 concentrations is possible as well as the existence of a single saddle node bifurcation.

In section 3.3 we have investigated the DK model and several approximations. Equation (3.15) shows that the value of $\bar{p}_{110}$ is not changed by this approximation.

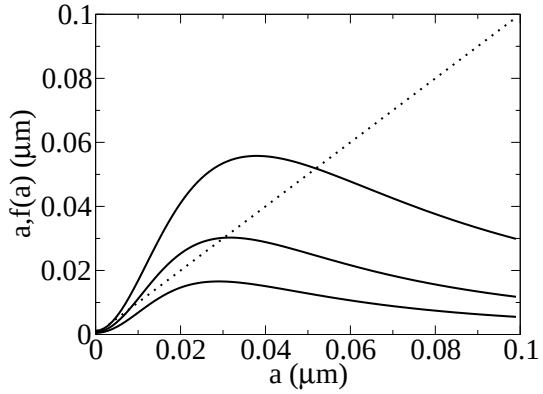

Figure 3.5: Stationary values of a given by the intersections of the bisection line (dotted) and the curve of f (solid). I increases from bottom to top. Parameter values are $d_1 = 0.13\mu M, d_2 = 3\mu M, d_3 = 0.9434\mu M, d_4 = 0.4133\mu M, k_p = 80s^{-1}, k_l = 0.002s^{-1}, k_c = 34500s^{-1}, E = 750\mu M, a_0 = 0.03\mu m, D = 40\mu m^2 s^{-1}$

Thus the above analysis remains valid and we proceed to the stability of the fixed points.

The linearization of equation (3.23) results in

$$\dot{y} = D\nabla_r^2 y - (k_l + k_p)y - \Theta(\bar{a} - r)k_c y + f_c \delta_D(r - \bar{a})\,. \tag{3.29}$$

We define $f_c := k_c(E - \bar{c})\delta a$. Note that the inner concentration field y_i is still restricted to $r \leq \bar{a}$. In linear order, the varying value of a is translated into an extra flux f_c at the rim of the stationary active area. Therefore the solution of (3.29) reads $y(r,t) = \exp(\omega t)u(r)$ with

$$u(r) = A\frac{\sinh(k_1 r)}{r}\Theta(\bar{a} - r) + B\frac{\exp(-k_2 r)}{r}\Theta(r - \bar{a}) \tag{3.30}$$

and

$$k_1 = \sqrt{\frac{k_l + k_p + k_c + \omega}{D}}\,, \quad k_2 = \sqrt{\frac{k_l + k_p + \omega}{D}}\,. \tag{3.31}$$

We used the boundary conditions $u'(0) = 0$ and $u(b) = 0$. The still unknown coefficients A and B are fixed by the continuity of u and the discontinuity of u' at $\bar{a}$. The latter is a direct consequence of the delta function $\delta_D(r - \bar{a})$ in equation (3.29). The continuity of u demands that

$$A\frac{\sinh(k_1\bar{a})}{\bar{a}} = B\frac{\exp(-k_2\bar{a})}{\bar{a}}\,, \tag{3.32}$$

whereas the discontinuity of u' requires

$$B\left[\frac{k_2\exp(-k_2\bar{a})}{\bar{a}} + \frac{\exp(-k_2\bar{a})}{\bar{a}^2}\right] + A\left[\frac{\cosh(k_1\bar{a})k_1}{\bar{a}} - \frac{\sinh(k_1\bar{a})}{\bar{a}^2}\right] - \frac{f_c}{D} = 0\,. \tag{3.33}$$

At first sight the two equations (3.32) and (3.33) do not represent a homogeneous system for the constants A and B. We will show that $f_c \propto u(r)$ which establishes homogeneity at second glance.

We start from equation (3.25). It holds for all models of the IP_3 receptor that we have discussed in section 3.3. For the lumped state model it takes the form

$$a = a_0 \frac{I}{I+d_1} p_{10} \sqrt[3]{4 - 3\frac{I}{I+d_1} p_{10}}\,. \tag{3.34}$$

It only depends on one gating variable, viz. p_{10}. Equation (3.7) entails that $\delta a \propto z_{10}$. Hence, the above statement is proven if $z_{10} \propto u(r)$. The solution for z_{10} follows from the matrix equation $\dot{x} = Mx$ with $x = (u, z_{00}, z_{01}, z_{10}, z_{11})^t$. The matrix M has the same form as in equation (3.8). Here, A_2 corresponds to the matrix in equation (3.24). The other two matrices degenerate to a vector and a differential operator as

$$B = (-a_5\bar{p}_{00} - a_6\bar{p}_{00}\,, a_6\bar{p}_{00} - a_5\bar{p}_{01}\,, a_5\bar{p}_{00} - a_6\bar{p}_{10}\,, a_5\bar{p}_{01} + a_6\bar{p}_{10})^t\,, \tag{3.35a}$$

$$A_1 = D\nabla_r^2 - (k_l + k_p + k_c)\,. \tag{3.35b}$$

The general discussion in section 3.2 has shown that all eigenvalues belonging to the gating variables are negative. Indeed, the eigenvalues for A_2 read

$$\{0, -b_5 - a_5 c, -b_6 - a_6 c, -b_5 - b_6 - a_5 c - a_6 c\}\,. \tag{3.36}$$

Consequently, we only have to take into account the mode from the dynamics of y. We obtain the eigenvector to the eigenvalue ω by solving the equation $Mx = \omega x$. The ansatz for y entails that $A_1 u = \omega u$ is always true because we assume that y is a solution to $\dot{y} = A_1 y$. This leads to a vanishing first line in the equation $Mx = \omega x$. It can be cast into the form $A_2(z_{00}, z_{01}, z_{10}, z_{11})^t = Bu$, so that $(z_{00}, z_{01}, z_{10}, z_{11})^t = A_2^{-1}Bu$. This proves $z_{10} \propto u(r)$. The inverse of A_2 exists because A_2 can be diagonalized.

It is convenient to introduce a new variable η by $\delta a =: \eta u$ for further computation. This leads to $f_c = k_c(E - \bar{c})\eta u$, see equation (3.29). Hence, the matrix M for the homogeneous system of equations for A and B is

$$M = \begin{pmatrix} \frac{\sinh(k_1\bar{a})}{\bar{a}} & -\frac{\exp(-k_2\bar{a})}{\bar{a}} \\ \frac{\cosh(k_1\bar{a})k_1}{\bar{a}} - \frac{\sinh(k_1\bar{a})}{\bar{a}^2} - \frac{k_c([E-\bar{c}(\bar{a})]\eta\sinh(k_1\bar{a})}{D\bar{a}} & \frac{k_2\exp(-k_2\bar{a})}{\bar{a}} + \frac{\exp(-k_2\bar{a})}{\bar{a}^2} \end{pmatrix}. \tag{3.37}$$

The system of equations possesses a non trivial solution only if the determinant of M equals zero. After multiplying the first line of equation (3.37) with $\bar{a}$ and

the second with $\bar{a}^2$ we find

$$\begin{aligned} 0 = \det M &= \sinh(k_1\bar{a})[k_2\bar{a}+1] - [\sinh(k_1\bar{a}) - \cosh(k_1\bar{a})k_1 a] \\ &\quad - \frac{k_c[E-\bar{c}(\bar{a})]\bar{a}\eta\sinh(k_1\bar{a})}{D} \\ &= k_2 + k_1\coth(k_1\bar{a}) - \frac{k_c[E-\bar{c}(\bar{a})]}{D}\eta\,. \end{aligned} \tag{3.38}$$

η can be computed explicitly for the lumped state model and takes the form

$$\eta = \frac{\kappa(\omega)}{1-\kappa(0)\frac{\partial\bar{c}}{\partial r}(\bar{a})} \tag{3.39}$$

with

$$\kappa(\omega) = \left[a_0 \frac{4(1-\bar{p}_{110})}{\sqrt[3]{(4-3\bar{p}_{110})^2}} \frac{\bar{p}_{110}}{\bar{c}} \left\{ \frac{d_5}{\frac{\omega}{a_5}+d_5+\bar{c}} - \frac{\bar{c}}{\frac{\omega}{a_6}+d_6+\bar{c}} \right\} \right]_{\bar{a}}. \tag{3.40}$$

The factor of the curly brackets stems from the derivative $\partial f/\partial p_{10}$. The eigenvector of ω leads to the expression in the curly brackets. Equations (3.38) to (3.40) determine the linear stability for the Ca^{2+} concentration. Thus, the whole stability analysis of the five variables $\{c, p_{00}, p_{01}, p_{10}, p_{11}\}$ could be reduced to a single algebraic equation. This is one of the great advantages of the model introduced in section 3.2.

We know from section 3.3 that the stationary value $\bar{p}_{110}$ does not depend on the approximation of the DK model. Calculating $\kappa(\omega)$ for the Li Rinzel model yields

$$\kappa^{LR}(\omega) = \left[a_0 \frac{4(1-\bar{p}_{110})}{\sqrt[3]{(4-3\bar{p}_{110})^2}} \frac{\bar{p}_{110}}{\bar{c}} \left\{ \frac{d_5}{d_5+\bar{c}} - \frac{\bar{c}}{\frac{\omega}{a_6}+d_6+\bar{c}} \right\} \right]_{\bar{a}}. \tag{3.41}$$

It is almost identical to equation (3.40). The only difference is the first denominator in the curly brackets. The absence of the term ω/a_5 originates from the adiabatic elimination of Ca^{2+} activation. The binding to the activating site is controlled by the rate constant a_5. Assuming that it is fast equals a very large value of a_5. Hence the fraction ω/a_5 tends to zero in this approximation.

If the system exhibits a zero eigenvalue bifurcation for a given pair $(\bar{a}, I)$ then $\omega = 0$ should solve equation (3.38). Indeed, using the identity

$$\frac{k_c}{D}\frac{E-\bar{c}(\bar{a})}{\bar{k}_2+\bar{k}_1\coth(\bar{k}_1\bar{a})} = \frac{\partial\bar{A}}{\partial a}(\bar{a})\frac{\sinh(\bar{k}_1\bar{a})}{\bar{a}} \tag{3.42}$$

equation (3.38) can be transformed to $1 = f'(\bar{a})$. This is one of the conditions for a saddle node bifurcation.

3.5 Results

Diffusion of calcium plays a central role for the selection of dynamic regimes of Ca^{2+} dynamics besides the dynamics of the IP_3 receptor. As Ca^{2+} binds to buffer proteins in the cytosol, its diffusion changes. Buffering leads to an effective diffusion coefficient of $40\mu m^2 s^{-1}$. However, buffers saturate at Ca^{2+} concentrations found in the vicinity of an open cluster. Then Ca^{2+} can diffuse with its own diffusion coefficient of $220 - 300\mu m^2 s^{-1}$ (Allbritton et al. 1992). Since we do not include buffers explicitly in our model we present results for $D = 40\mu m^2 s^{-1}$ and $D = 220\mu m^2 s^{-1}$.

The original DK model is based on a continuous distribution of IP_3 receptors. The most prominent feature of the Ca^{2+} dynamics are two Hopf bifurcations bounding an oscillatory regime. We test whether this property is conserved when going from the spatially continuous description to a discrete model. To this aim we rescale the flux density with a typical cluster spacing R and a representative cluster radius a_0 while keeping the total flux constant, i.e. $k_c = k_c^{DK} R^3/a_0^3$. The resulting k_c of $3\ 10^5 s^{-1}$ which agrees well with the realistic values in chapter 1 leads to a loss of the oscillatory regime. We find a single stationary state for all IP_3 concentrations that is linearly stable. Decreasing the flux density by several orders of magnitude and thus approaching the original value does not restore oscillations. This holds because gradients still prevail. This is similar to findings in (Sneyd and Sherrat 1997).

However, transforming a spatially continuous model to a system with discrete sources requires more than rescaling the flux density. The work by DeYoung and Keizer describes spatially averaged Ca^{2+} concentrations. They are much lower than those experienced by IP_3Rs at the mouth of a cluster. Therefore we have to adapt the constants of Ca^{2+} binding. For the inhibitory process we use $d_2 = 3\mu M$ in agreement with recent measurements (Adkins and Taylor 1999) (Mak et. al found dissociation constants up to 45μM but based on a specific model (Mak et al. 2003)). According to the experiments in (Adkins and Taylor 1999) the coefficients for binding to the inhibiting site a_2 and a_4 are both set to $0.2\,(\mu M s)^{-1}$. The binding rate to the activating site can be evaluated from puff frequencies (Yao et al. 1996). This implies $a_5 \geq 1\,(\mu M s)^{-1}$. Assays of the dissociation constant for Ca^{2+} activation yield values from 77nM to 309nM (Mak et al. 1998, Mak et al. 2001, Ramos-Franco et al. 1998). We chose $d_5 = 0.823\mu M$ which is motivated by the results depicted in figure 3.6. It shows the dynamical regimes of the model in dependence on d_5 and I. Oscillations occur for larger d_5 values only. Since we would like to analyze oscillations and evaluate them in the light of experimental results, we chose this value.

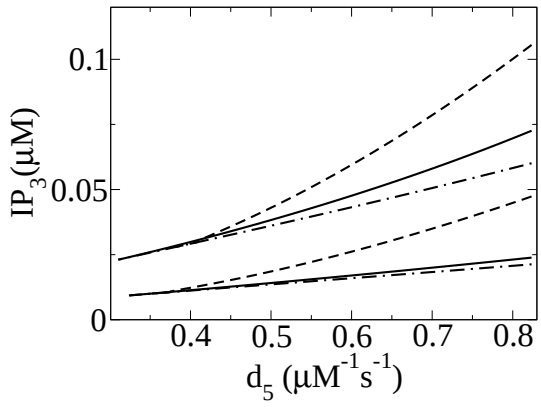

Figure 3.6: IP_3 concentration of the saddle node bifurcations (solid and chain dotted) and the Hopf bifurcation (dashed) in dependence on d_5. Upper group $D = 220\mu m^2 s^{-1}$, lower group $D = 40\mu m^2 s^{-1}$ Parameter values are $d_1 = 0.13\mu M, d_2 = 3\mu M, d_3 = 0.9434\mu M, d_4 = 0.4133\mu M, k_p = 80s^{-1}, k_l = 0.002s^{-1}, k_c = 34500s^{-1}, E = 750\mu M, a_0 = 0.03\mu m, a_2 = a_4 = 0.2(\mu Ms)^{-1}, a_5 = 1(\mu Ms)^{-1}$.

There are two saddle node bifurcation lines terminating in a cusp. A Hopf bifurcation occurs above the two saddle node bifurcations. Oscillations can be found at IP_3 concentrations bounded by the Hopf bifurcation and a bifurcation occurring between the Hopf bifurcation and the lower saddle node bifurcation. The type of this bifurcation is still under investigation but is probably homoclinic. Fig. 3.6 demonstrates that oscillations do not occur at values of d_5 suggested by measurements, since the activation process completely saturates at the concentration values occurring at an open channel. Hence, changing dissociation constants of the original DK model to larger experimentally supported values did not restore oscillations. However, even if the cluster dynamics oscillated, these oscillations would not be the experimentally observed ones. To demonstrate that, we need to choose parameter values allowing for oscillations. Therefore we use a value of k_c large enough to provide realistic concentration values at the releasing cluster (i.e. larger than 25μM), if a large fraction of channels is open, but small enough to still see a variety of dynamic regimes, and a value of d_5 allowing for oscillations. The values of all parameters are given in the caption of Fig. 3.6. Stationary states with these parameter values are presented in Fig 3.7. There is just a single stationary state for almost all IP_3 concentrations. An oscillatory regime exists close to the bistable area. We did not find limit cycles where the stationary state is stable. Hence, the discrete DK model does not have an oscillatory regime of experimentally relevant extension.

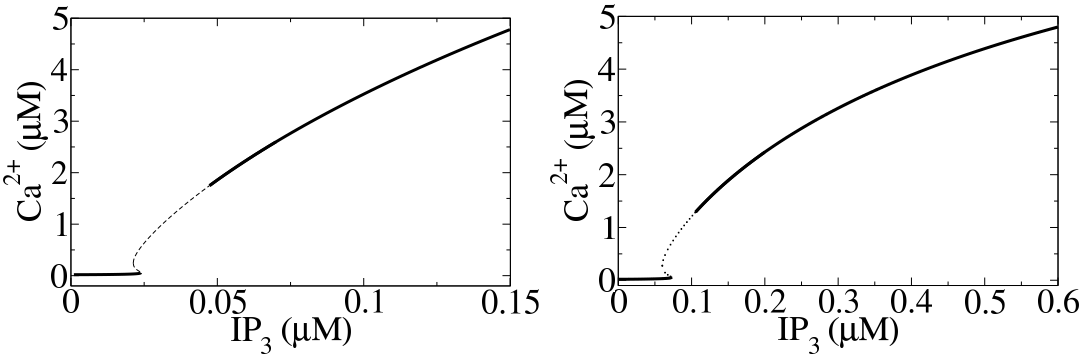

Figure 3.7: Stationary values of the Ca^{2+} concentration for $D = 40\mu m^2 s^{-1}$ (left) and $D = 220\mu m^2 s^{-1}$ (right). Solid lines denote linearly stable fixed points, dotted linearly unstable points. Parameters as in Fig 3.6 and $d_5 = 0.8234\mu M, a_2 = a_4 = 0.2(\mu M s)^{-1}, a_5 = 1(\mu M s)^{-1}$.

Besides the size of the oscillatory regime, there is another observation suggesting that these oscillations are not the experimentally observed global oscillations in cells. Fig.3.8 shows oscillations of the Ca^{2+} concentration. The initial transient illustrates that realistic concentration values at the cluster are reached. The amplitude of the oscillations at the releasing cluster is much smaller than the initial peak. It is even more damped down to less than 1nM in a distance of 1.6μm from the cluster. That bulk amplitude is too small to represent the observed global oscillations.

The oscillation amplitude at the releasing cluster is in the order of magnitude of the dissociation constant of the inhibitory process. The latter is in the range of a few 100nM to several μM. The amplitude of the oscillations had to be expected for such a sinusoidal oscillation since changes of concentrations far above or below the dissociation constant do not exert a feedback on the dynamics. The reason lies in the equations that govern the dynamics: they are Hill equations. A typical plot is shown in figure 3.9. It depicts the function $hi(c) := [c/(c + d_2)]^3$ for the inhibitory dissociation constant d_2. The term $c/(c + d_2)$ is referred to as a Hill equation with Hill coefficient 1 because c and d_2 enter with the exponent 1. The expression $c/(c + d_2)$ describes binding and unbinding of Ca^{2+} to a single binding site. The function $hi(c)$ represents the probability that three ions bind independently to inhibiting binding sites. It is motivated by the assumption that the four subunits of the IP_3 receptor do not interact. Binding at one subunit does not interfere with other subunits. We see from figure 3.9 that hi saturates for high concentration values. They are in the order of magnitude that reached at an open cluster. Therefore, a transient peak as in figures 3.8 and 3.10 leads to a saturation of the control of the IP_3R by Ca^{2+} and is the reason for the small

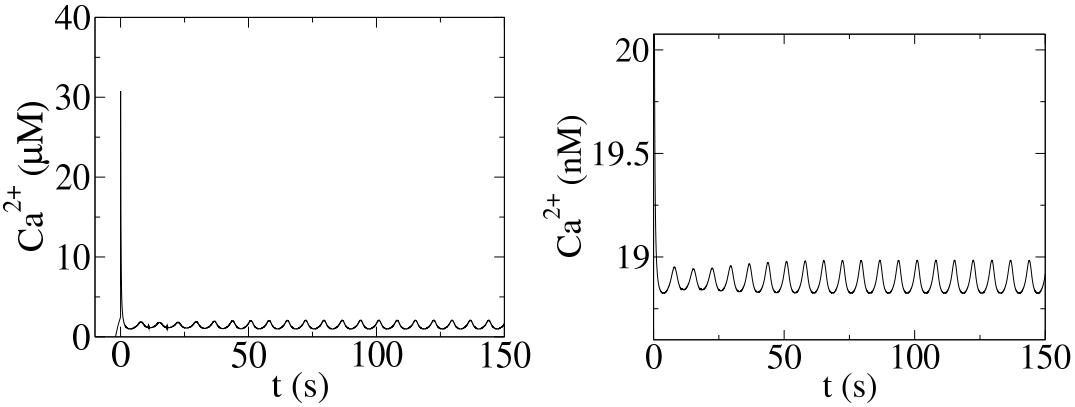

Figure 3.8: Oscillation of the Ca^{2+} concentration at a distance $r = 0\mu m$ (left) and $r = 1.588\mu m$ (right) from the center. Note the difference in the order of magnitude for the amplitude and mean. Parameters as in Fig 3.7 and $D = 40\mu m^2 s^{-1}$.

oscillatory regimes and amplitudes.

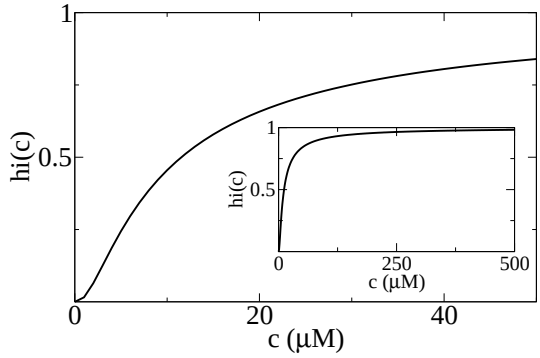

Figure 3.9: Typical dependence of a hill equation $hi(c)$ on the concentration c. Inset shows saturation for large values of c.

That amplitude in the range of dissociation constants - and the small bulk amplitudes - will apply to other models than the DK model, too. Hence, not only is the oscillatory regime too small in parameter space to be the experimentally observed regime but also is it found at unphysiological values only. Moreover the bulk amplitudes are too small.

The results presented so far have been obtained for parameters that are specific for IP_3 induced Ca^{2+} liberation from the ER. In the remainder of this section we go beyond this range. We investigate the model behavior for different parameters that might be significant for membrane bound reactions. In a first step we speed up binding to the activating Ca^{2+} site by using a ten fold higher value

for a_5. We leave the dissociation constants unchanged, so that the the values of the stationary states do not change. The oscillations that arise via the Hopf bifurcation are depicted in figure 3.10. The pattern resembles those of figure 3.8. Upon increasing IP_3, the system responds with a huge spike of release and finally settles into small amplitude oscillations. The large value of the initial transient is a direct consequence of the large value of a_5. It facilitates channel opening. Note the logarithmic scale in the left panel of figure 3.10.

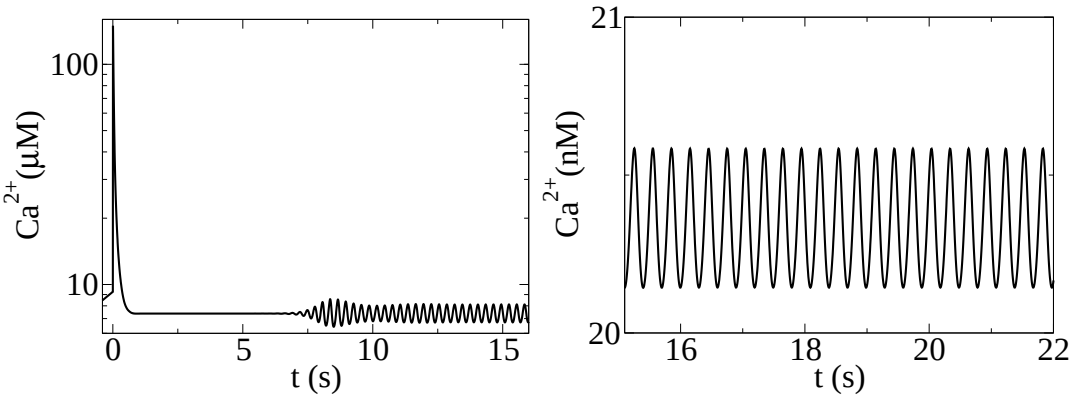

Figure 3.10: Oscillations of the Ca^{2+} concentration at a distance $r = 0\mu m$ (left) and $r = 1.588\mu m$ (right) from the center. Note the difference in the order of magnitude for the amplitude. Parameters as in Fig 3.6 and $D = 40\mu m^2 s^{-1}, a_5 = 10(\mu M s)^{-1}$.

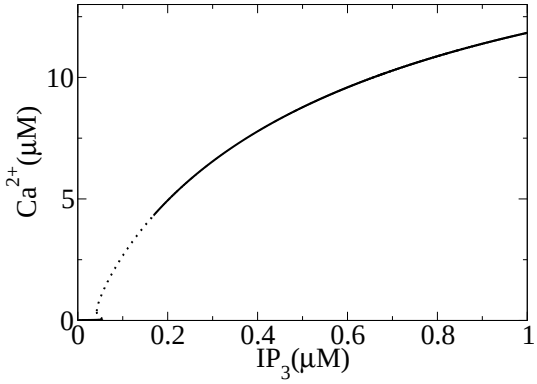

Figure 3.11: Stationary values of the Ca^{2+} concentration for $D = 40\mu m^2 s^{-1}$. Solid lines denote linearly stable fixed points, dotted linearly unstable points. Parameters as in Fig 3.6 and $d_5 = 1.6468\mu M$.

Figure 3.11 shows that the structure of the bifurcation diagram does not change with a higher value of the activating dissociation constant, cp. 3.7. There is a

single fixed point for almost all IP_3 concentrations. Stable limit cycles exist close to the bistable area. They only extend to IP_3 concentration where the upper branch is unstable. Hence, we can exclude the possibility that oscillations arise via other bifurcations than the Hopf bifurcation. Thus we again find a very small band of IP_3 concentrations in which the system oscillates. The oscillations behave in the same way as described above.

Finally we test the influence of the binding rate constant for Ca^{2+} activation a_5 and of the binding rate for Ca^{2+} inhibition a_2 on the stationary states. The concentration values of the stationary states are conserved since we do not change the dissociation constants. Whereas the saddle node bifurcations stay in place the Hopf bifurcation is shifted. The Hopf bifurcation moves toward the left saddle node bifurcation, when we increase the rates for the inhibitory processes. Figure 3.12 displays the difference of the IP_3 concentrations values of the Hopf bifurcation and the left saddle node bifurcation. It monotonically decreases to zero with higher values of a_2. Hence the oscillatory regime shrinks for stronger inhibition. Measurements by Taylor suggest that inhibition is much fast than usually assumed in modeling (Adkins and Taylor 1999). That again lends support to our results that the oscillatory regime is not present in discrete models. The opposite effect occurs for Ca^{2+} activation. An increment of a_5 (while keeping d_5 constant) shifts the Hopf bifurcation to higher IP_3 concentration.

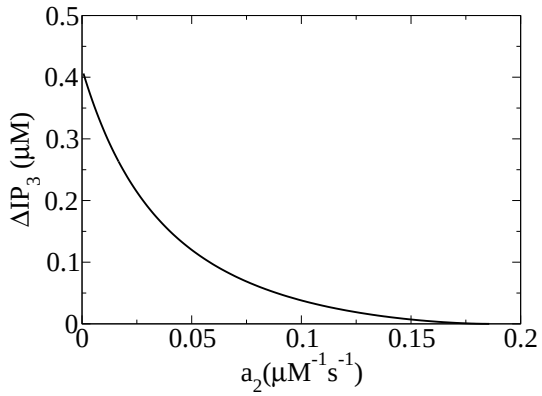

Figure 3.12: Difference between the IP_3 concentration of the Hopf bifurcation and the left saddle node bifurcation in dependence on the binding rate for inhibition a_2. Parameters as in Fig. 3.14 and $D = 40\mu m^2 s^{-1}, a_2 = a_4$.

Oscillations do not always disappear as simply as in a (putative) homoclinic bifurcation. The results in figure 3.13 illustrate a period doubling sequence found while approaching the lower saddle node bifurcation. The left panel shows a period-2 example and the right one a period-4 example. Higher periods occur,

too. As in the previous case the system only oscillates when the upper branch is unstable thus leading to a small oscillatory regime. The oscillations are again considerably damped at a distance of $1.6\mu m$. Whether this period doubling sequence leads to chaos is subject of ongoing investigations.

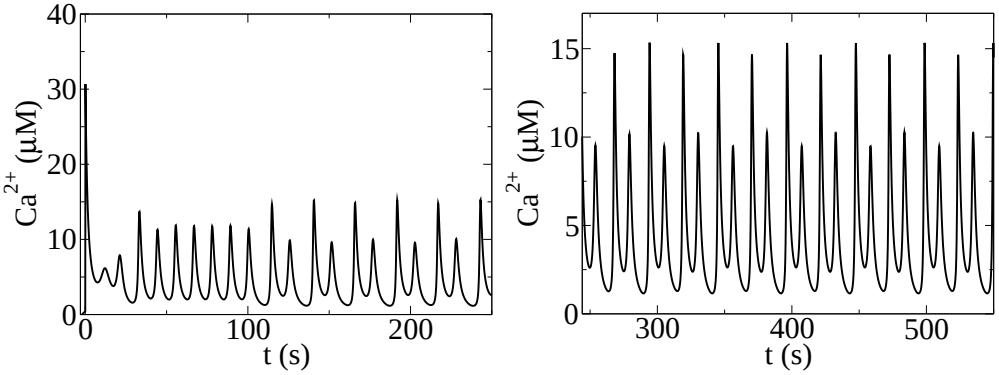

Figure 3.13: Oscillations of the Ca^{2+} concentration at $r = 0\mu m$ for different values of the IP_3 concentration. At $t = 100s$, we decrease I from 0.22μM to 0.218μM (left panel), whereas $I = 0.215\mu$M for all times (right panel). Parameters as in Fig 3.14 and $D = 50\mu m^2 s^{-1}$.

A different structure of the bifurcation diagram can be found with parameter values like those used in figure 3.14. For $D = 40\mu m^2 s^{-1}$ we find again two saddle node bifurcations and a Hopf bifurcation. This is similar to the results above. However, increasing the diffusion coefficient changes the topology of the bifurcation diagram. A value of $D = 220\mu m^2 s^{-1}$ yields one saddle node bifurcation only. It creates an area with three stationary states extending infinitely toward high IP_3 concentration values. A transition from the lower branch of stationary points to the upper one cannot be achieved by increasing IP_3 concentration slowly. It has to be initiated by a perturbation of the system which could as well be a step increase of IP_3 .

These two examples illustrate that for a given set of parameters, diffusion can essentially influence the dynamic behavior. Generally the impact of diffusion on the fixed points can be deduced from the derivative of the stationary Ca^{2+} concentration $\bar{c}'$. Here the prime refers to the derivative with respect to D. It can be simplified to

$$\frac{1}{\zeta}\bar{c}'(a) = \bar{k}_1'(\bar{k}_2 a + 1)\left\{\bar{k}_1 - \frac{\sinh(2\bar{k}_1 a)}{2a}\right\} + \bar{k}_2'\left\{\frac{\sinh(2\bar{k}_1 a)}{2}\bar{k}_1 - \frac{\sinh^2(\bar{k}_1 a)}{a}\right\} \tag{3.43}$$

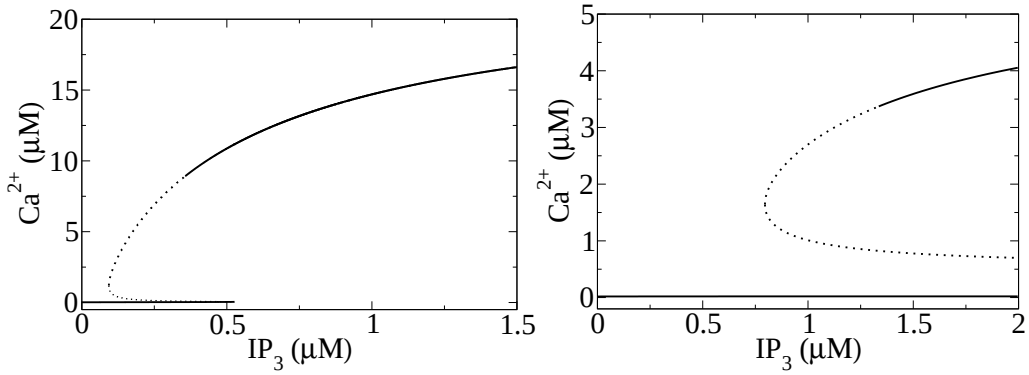

Figure 3.14: Stationary values of the Ca^{2+} concentration for $D = 40\mu m^2 s^{-1}$ (left) and $D = 220\mu m^2 s^{-1}$ (right). Solid lines denote linearly stable fixed points, dotted linearly unstable points. Parameter values are $d_1 = 0.13\mu M, d_2 = 12.588\mu M$, $d_3 = 0.9434\mu M, d_4 = 1.7346\mu M, d_5 = 2.4702\mu M, k_p = 80s^{-1}, k_l = 0.002s^{-1}$, $k_c = 700s^{-1}, E = 750\mu M, a_0 = 0.11\mu m, a_2 = a_4 = 0.0167(\mu Ms)^{-1}, a_5 = 0.667(\mu Ms)^{-1}$.

with

$$\zeta = \frac{k}{\left(\cosh(\bar{k}_1 a)\bar{k}_1 + \sinh(\bar{k}_1 a)\bar{k}_2\right)^2}\,. \tag{3.44}$$

As $\bar{k}_i' = -\bar{k}_i/(2D)\,, i = 1, 2$ we immediately arrive at $\bar{c}'(a) < 0$. This entails that for any $\Delta > 0$ there exists an $\alpha > 0$ so that $f_{D+\Delta}(a + \alpha) = f_D(a)$. That can be seen as follows. We choose an arbitrary, but fixed value a_0 of a and one curve $f(a)$ in figure 3.5. Upon increasing D from D_1 to D_2, the value of the Ca^{2+} concentration decreases from $c_1 = c(D_1)$ to $c_2 = c(D_2)$ at a_0. Figure 3.16 shows the stationary value $\bar{p}_{110}$ in dependence on the Ca^{2+} concentration c. Note the biphasic behavior of the probability which agrees with experimental data (Bezprozvanny et al. 1991). Lowering the Ca^{2+} concentration from c_1 to c_2 equals a move toward the left on the abscissa. This amounts to a step from a_0 to a smaller value of a in figure 3.5 due to the following reason. The function $x \mapsto x\sqrt[3]{4 - 3x}$ is strictly increasing. Hence $f(c) = f(p(c))$ has the same shape as $\bar{p}_{110}(c)$ in figure 3.16. Using the radius a in f via $c = \bar{c}(a)$ does not change the form of the curve of f because $\bar{c}(a)$ is strictly increasing with respect to a. These two one-to-one mappings assure that lowering c corresponds to decreasing a. Consequently, the value of f_{D_2} at a_0 equals a value of f_{D_1} for a smaller value of a. This proofs the above assertion. The geometric interpretation is a stretching of f to the right upon increasing the diffusion coefficient. Figure 3.15 clearly illustrates this behavior. It shows $f(a)$ for the two diffusion constants $D = 40\mu m^2 s^{-1}$ and $D = 220\mu m^2 s^{-1}$. In the left panel we have chosen $I = 0.3\mu m$. There are 3

stationary values for $D = 40\mu\text{m}^2 s^{-1}$ and one for $D = 220\mu\text{m}^2 s^{-1}$. This is in agreement with the bifurcation diagram in figure 3.14. The right panel shows the stationary values for such a high value of I that all IP_3 dependent processes have saturated. This happens because the IP_3 dynamics is controlled by Hill type expressions. In comparison with the left panel we see the upward shift of $f(a)$ for a fixed diffusion constant. This coincides with the general discussion in section 3.2. There is only one stationary value for $D = 40\mu\text{m}^2 s^{-1}$ as we have moved beyond the right saddle node bifurcation in figure 3.14. Contrary three fixed points occur for $D = 220\mu\text{m}^2 s^{-1}$. The saturation of the IP_3 dynamics induces that the number of stationary states will not change if I increases. This explains the bifurcation diagram in figure 3.14.

The exact effect of increasing D on a given stationary point differs. We illustrate it with the fixed point of high Ca^{2+} concentration. It corresponds to the right intersection of f and the bisection line in the right panel of figure 3.15. Elevating D leads to a higher value of $\bar{a}$ for the chosen IP_3 concentration. On contrast, increasing D for $I = 0.3\mu\text{M}$ results in the disappearance of the fixed point. The system changes from a bistable regime for low D to a monostable regime for large D. This manifests again that diffusion essentially determines the dynamics of membrane bound reactions.

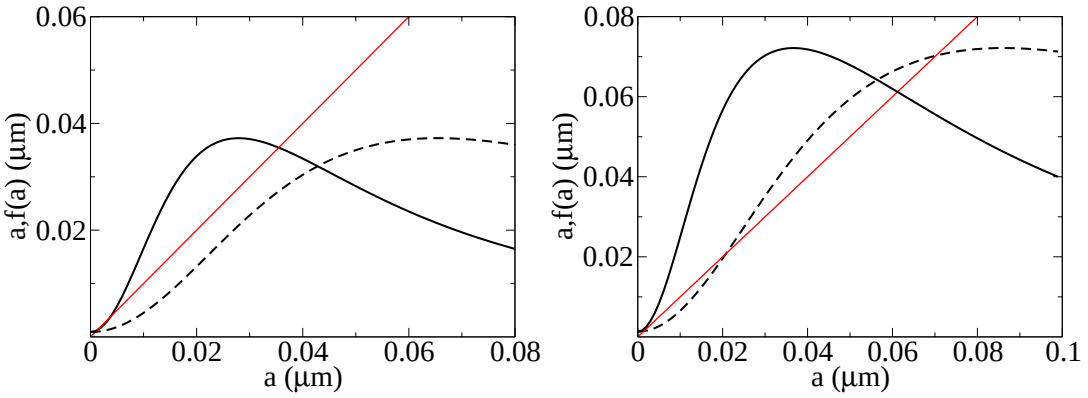

Figure 3.15: Stationary values of a given by the intersection of the bisection line (red) and the curves of f (black) for $D = 40\mu m^2 s^{-1}$ (solid) and $D = 220\mu m^2 s^{-1}$ (dashed) for different values of I. Left panel $I = 0.3\mu\text{M}$, right panel $I = 200\mu\text{M}$. Parameters as in figure 3.14.

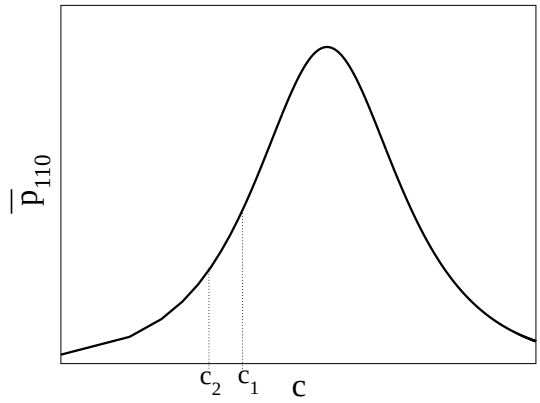

Figure 3.16: Stationary values of the probability p_{110} in dependence on c. Note the biphasic behavior. See text for details.

3.6 Conclusion

We have presented an extended study of a new modeling concept for systems in which diffusive species react with immobile partners. The immobile reaction partners are confined to small clusters. Our approach to describe the cluster dynamics is always applicable when the diffusion length is much larger than the cluster size. We applied the above method to the dynamics of intracellular calcium mediated by IP_3 receptors. The spatial restriction of the Ca^{2+} flux led to the disappearance of Ca^{2+} oscillations computed in spatially continuous models. The enlarged values of the Ca^{2+} concentration at the cluster resulted in a single linearly stable state. The oscillatory regime was not restored by decreasing the channel flux constant k_c. Hence, the strong impact of spatial gradients on dynamic regimes will most likely apply as well to localized reactions generating much smaller gradients than the gradients around a releasing Ca^{2+} channel.

At dissociation constants d_5 suggested by measurements the Ca^{2+} dynamics is monostable. But even if Ca^{2+} oscillates, these are not the oscillations seen in experiments. Two observations led to this conclusion. Firstly, the range of IP_3 concentrations providing oscillations is too small. Secondly, the amplitude as well as the mean of the oscillations are already considerably damped in a distance of $1.6\mu m$ from the cluster. Thus they cannot represent the global Ca^{2+} oscillations seen in experiments. The spatial damping of the oscillations applies to each reaction producing a species consumed or buffered in the cytosol. The damping will depend on the diffusion length resulting from this reaction diffusion process.

Our results contribute to recent findings in which the stochastic dynamics of a system differs essentially from the deterministic description. A comparison

of the bifurcation scheme of the deterministic Li-Rinzel model with simulations of its stochastic counterpart demonstrated that the deterministic regime cannot be concluded from the stochastic behavior (Jung and Shuai 2001, Shuai and Jung 2002b). Another example is array enhanced coherence resonance where stochasticity can induce global oscillations in non-oscillatory systems (Coombes and Timofeeva 2003).

The stochasticity of intracellular Ca^{2+} dynamics is caused by the stochastic binding and unbinding of IP_3 and Ca^{2+} to the small number of receptor molecules. Fluctuations cause spontaneous release in a single cluster. That leads to a release spike like the initial spikes in figures 3.8, 3.10 and 3.13. Such a large amplitude event can lead to the opening of neighboring clusters and finally via a nucleation process to a wave traveling through the whole cell. If that occurs repeatedly it leads to an oscillation-like process (Falcke 2003b). Nucleation may occur at different spots in the cell essentially at the same time, when the IP_3 concentration is high (Falcke 2003b). Thus, the amplitude of the initial spike is responsible for the amplitude of the oscillations.

Oscillations might as well be introduced by additional feedback, e.g. a Ca^{2+} feedback on IP_3 production or the filling state of the endoplasmic reticulum. Our findings suggest that the initiation of global Ca^{2+} release would still occur by wave nucleation since the subsystem Ca^{2+} dynamics would not undergo an instability of the local dynamics. The additional feedbacks would modulate the nucleation probability periodically.

It will be interesting to learn from future research, whether this pattern of the interplay between localization and fluctuations can be transferred to other intracellular systems.